改善된 HEMT 非線型 서브임계電壓 領域모델

(Improved Nonlinear Subthreshold Region Model For HEMTs)

金 榮 民

<ABSTRACT>

Closed form solution of nonlinear 2−DEG concentration formula is proposed. This allows us to model continuous 2−DEG charge concentration as the function of gate voltage covering subthreshold region of the I−V curves.

Comparisons of the Ids−Vgs characteristics and transconductance with the measured data were performed to show the accuracy of the proposed model. This way we have completely closed form I−V characteristics in subthreshold, triode and saturation region incorporating accurate charge control mechanism for HEMTs.

I. Continuous Nonlinear 2−DEG Charge Control Model

Using the Fermi−Dirac statistics with triangular potential well approximation, 2−DEG concentration n_s can be written as

$$n_s = D_s \frac{KT}{q} \left\{ (1+e^{\frac{q(E_{Fi}-E0)}{KT}})(1+e^{\frac{q(E_{Fi}-E1)}{KT}}) \right\} \cdots\cdots (1)$$

where E_{Fi} represents Fermi level, D_s is the density of states, $E0=\gamma_0 n_s^{2/3}$ and $E1=\gamma_1 n_s^{2/3}$ are the positions of first two allowed energy levels in the triangular potential well[1]. If we solve E_{Fi} as the function of n_s

$$E_{Fi}=KT\ln\left\{-\frac{1}{2}\left(e^{\frac{E0}{KT}}+e^{\frac{E1}{KT}}\right)+\left(\frac{1}{4}\left(e^{\frac{E0}{KT}}+e^{\frac{E1}{KT}}\right)^{2}+\left(e^{\frac{n_s}{DKT}}-1\right)e^{\frac{(E0+E1)}{KT}}\right)^{\frac{1}{2}}\right\} \quad \cdots\cdots\cdots\cdots (2)$$

Eq.2 can be rearranged as

$$E_{Fi}=KT\ln\left\{-\frac{1}{2}\left(e^{\frac{E0}{2KT}}-e^{\frac{E1}{2KT}}\right)^{2}e^{\frac{E0+E1}{2KT}}+\left[\frac{1}{4}\left(e^{\frac{E0}{KT}}-e^{\frac{E_1}{KT}}\right)^{2}+e^{\frac{(\frac{n_s}{D_s}+E0+E1)}{KT}}\right]^{\frac{1}{2}}\right\} \quad \cdots\cdots\cdots\cdots (3)$$

Since

$$\left(e^{\frac{E0}{KT}}-e^{\frac{E1}{KT}}\right)^{2} << e^{\frac{(E0+E1)}{KT}}$$

and

$$\left(e^{\frac{E0}{2KT}}-e^{\frac{E1}{2KT}}\right)^{2} << e^{\frac{(E0+E1)}{2KT}}$$

E_{Fi} can be simplified as

$$E_{Fi}=\frac{E0+E1}{2}+KT\ln\left(e^{\frac{n_s}{2KTD_s}}-1\right)\cdots\cdots\cdots(4)$$

In order to validate the approximation taken above, we compared Eq.4 with the original formula given Eq.2 in Fig.1 using temperature as a parameter. The '*' represents Eq. 4 and the solid line represents Eq. 2. We notice that this expression produces little error in wide range of tempereture and 2-DEG concentration. However this expression is still not suitable for a losed expression for n_s. The Talyor series expansion of Eq. 4 with respect to E_{Fi} in the vicinity of $n_s=n_{so}$ can be written as

$$ns=A\ E_{Fi}^{2}+B\ E_{Fi}+C \quad \cdots\cdots\cdots\cdots (5)$$

where

$$A=\frac{1}{2}\frac{d^{2}n_s}{dE_{Fi}^{2}}\Big|\, n_{so}$$

$$B=\frac{dn_s}{dE_{Fi}}\Big|\, n_{so}-E_{Fi}(n_{so})\frac{d^{2}n_s}{dE_{Fi}^{2}}\Big|\, n_{so}$$

$$C=n_{so}-E_{Fi}(n_{so})\frac{dn_s}{dE_{Fi}}\, n_{so}+\frac{1}{2}E_{Fi}(n_{so})^{2}\frac{d^{2}n_s}{dE_{Fi}^{2}}\, n_{so}$$

$$\frac{dn_s}{dE_{Fi}}=\left(\frac{dE_{Fi}}{dn_s}\right)^{-1}=\left\{\frac{r_0+r_1}{3}n_s^{-\frac{1}{3}}+\frac{e^{\frac{n_s}{2KTD_s}}}{2D_s\left(e^{\frac{n_s}{2KTD_s}}-1\right)}\right\}^{-1}=G(n_s)\cdots(6)$$

$$\frac{d^{2}n_s}{dE_{Fi}^{2}}=\frac{dn_s}{dE_{Fi}}\left(\frac{d}{dn_s}\left(\frac{dn_s}{dE_{Fi}}\right)\right)=\left\{\frac{r_0+r_1}{9}n_s^{-\frac{4}{3}}+\frac{e^{\frac{n_s}{2KTD_s}}}{4KTD_s^{2}\left(e^{\frac{n_s}{2KTD_s}}-1\right)^{2}}\right\}G(n_s)^{3}$$

$E_{Fi}(n_{so})$ can be evaluated from Eq. 4. Fig. 1 shows the comparison of the exact Fermi-level(Eq. 2) using the Fermi-Dirac statistics with the Taylor expansion represented by dashed line. Here n_{so} is taken to have the value of $3\times10^{15}\ m^{-2}$ for best reproduction of exact curve. The values of A, B and C at 300 K are 1.877674×10^{17}, 3.815598×10^{16}, and 2.330128×10^{15} respectively.

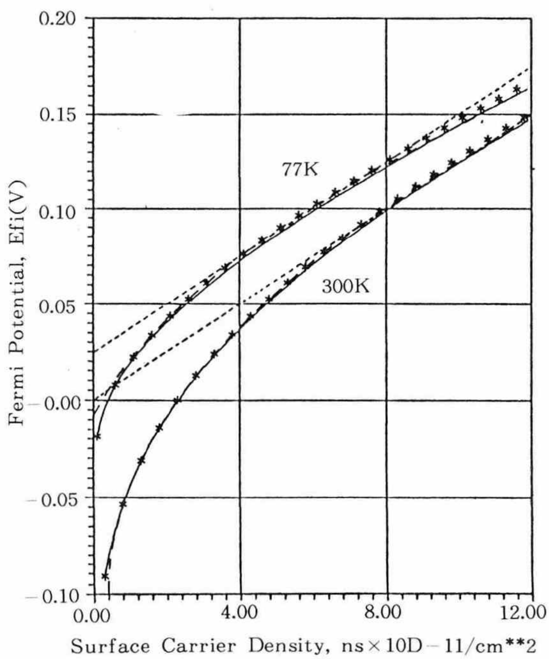

Fig. 1

When there is no current flow along the channel, surface electron charge can be expressed as

$$n_s = \frac{k_0\varepsilon_0}{qd}\left(V_g - V_{th} - \frac{E_{Fi}}{q}\right) \cdots\cdots\cdots\cdots\cdots (7)$$

where $d = d_d + d_i$ and V_{th} represents a threshold voltage that can be expressed as

$$V_{th} = \phi_b - V_{p2} - \frac{\Delta E_c}{q} \cdots\cdots\cdots\cdots\cdots\cdots\cdots (8)$$

where ϕ_b is the Shottkey barrier potential between AlGaAs and Al, ΔE_c the conduction band discontinuity and $V_{p2} = qN_d d_d^2/2\varepsilon_o$.

Elimination of n_s from Eq.5 and 7 results in an expression for the Fermi level as

$$E_{Fi}(V_g) = \frac{B + \frac{k_0\varepsilon_0}{qd}}{2A} + \left(\left(\frac{\frac{k_0\varepsilon_0}{qd}}{2A}\right)^2 + \frac{1}{A}\left[C - \frac{k_0\varepsilon_0}{qd}(V_g - V_{th})\right]\right)^{\frac{1}{2}} \cdots (9)$$

From Eq.7 and 9, surface charge density can be expressed as

$$n_s = \frac{k_0\varepsilon_0}{qd}\left\{V_g - V_{th} + \frac{B + \frac{k_0\varepsilon_0}{qd}}{2A} - \left(\frac{B + \frac{k_0\varepsilon_0}{qd}}{2A} - \frac{1}{A}\left[C - \frac{k_0\varepsilon_0}{qd}(V_g - V_{th})\right]\right)^{\frac{1}{2}}\right\} \cdots (10)$$

This equation represents surface charge density as the continuous function of gate voltage covering subthreshold to linear region of I−V curves.

$$d_c = \frac{k_0\varepsilon_0 dE_{Fi}}{q^2\, dn_s} = \frac{k_0\varepsilon_0}{q^2} G^{-1}(n_s) \cdots\cdots\cdots\cdots (11)$$

where n_s is defined in Eq.7. This way one obtains the channel thickness as the function of gate voltage.

Ⅱ. I−V Curves for Triode Region

When a drain voltage is applied, the channel charge can be expressed as

$$n_s = \frac{k_0\varepsilon_0}{qd}\left\{V_g - V_{th} - \frac{E_{Fi}(V_g)}{q} - (1-f)V_c\right\} \cdots\cdots\cdots (12)$$

where f was incorporated to account for the transition section V_c being the channel voltage. Then channel current can be written as

$$I = qZn_s\nu \cdots\cdots\cdots\cdots\cdots\cdots\cdots\cdots\cdots\cdots\cdots\cdots\cdots\cdots (13)$$

If we consider the Troffimenkoff type of field−dependent mobility, where the electron velocity is expressed as

$$\nu = \mu\varepsilon = \frac{\mu_0\varepsilon}{1 + \varepsilon/\varepsilon_c} \cdots\cdots\cdots\cdots\cdots\cdots\cdots (14)$$

where μ_0 denotes low−field mobility of electrons and ε_c the critical electric field. Then the drain current can be expressed as

$$I_D = \beta\left(\frac{\varepsilon}{1 + \varepsilon/\varepsilon_c}\right)\left(V_{off} - (1-f)V_c\right) \cdots\cdots\cdots\cdots\cdots (15)$$

where

$$\beta = \frac{k_0\varepsilon_0 Z\mu_0}{d}$$

and

$$V_{off} = \left\{V_g - V_{th} - \frac{E_{Fi}(V_g)}{q}\right\}$$

where Z is a channel width. By integrating Eq. 13 from x=0 to x=L, Eq. 15 the channel current can be expressed as

$$I_D = \frac{\beta}{L + V_D/\varepsilon_c}\left(V_{off}V_D - \frac{1}{2}(1-f)V_D^2\right) \cdots\cdots\cdots (16)$$

where V_D is the drain voltage.

Ⅲ. I−V Curves for Saturation Region

Taking transition section into account, a three-section model which is shown in Fig. 2. can be established. This figure corresponds to the case when applied drain voltage is well above saturation voltage. In this figure, d_c and d_s represent the channel thicknesses of GCA section and saturated section respectively. The electron velocity at the saturated section is assumed to be in full saturation without appreciable error. Then V_P can be calculated from the expression for the triode region of I-V curves. From Eq.16

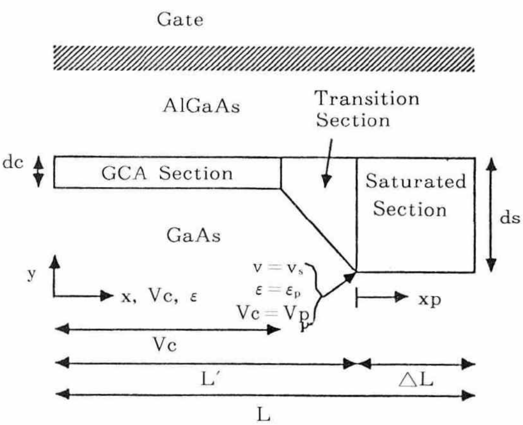

Fig. 2

$$I_p=\frac{\beta}{L+V_p/\varepsilon_c}\left(V_{off}V_p-\frac{1}{2}(1-f)V_p^2\right)\cdots\cdots\cdots\cdots\cdots(17)$$

Also from Eq. 15

$$I_p=\beta\left(\frac{\varepsilon_p}{1+\varepsilon_p/\varepsilon_c}\right)\left(V_{off}-(1-f)V_p\right)\cdots\cdots\cdots\cdots(18)$$

where ε_p is the electric field at the boundary between the saturated section and the transition section. Elimination of I_p from Eqs. 17 and 18 to solve for V_p leads to

$$V_p=-\frac{\varepsilon_c(V_{off}+\varepsilon_p L(1-f))}{(1-f)\ (\varepsilon_p-\varepsilon_c)}+\sqrt{\left(\frac{\varepsilon_c(V_{off}+\varepsilon_p L(1-f)}{(1-f)(\varepsilon_p-\varepsilon_c)}\right)^2+\frac{2V_{off}\ \varepsilon_c\varepsilon_p L}{(-f)\ (\varepsilon_p\varepsilon_c)}}\cdots(19)$$

Assuming full velocity saturation in the saturated section, i.e., $\nu=\nu_s$, and neglecting the component of n_s normal to the hetero-interface in the saturated section, Poisson equation can be reduced to

$$\frac{d^2V_c}{dx^2}=\frac{I_D}{k_0\varepsilon_0 Zd_s\nu_s}\cdots\cdots\cdots\cdots\cdots\cdots(20)$$

where

$$\nu_s=\mu_0\varepsilon_c$$

and

$$K=\frac{1}{k_0\varepsilon_0 Zd_s\ \nu_s}$$

Using the saturation current expression derived in[7]

$$I_D=I_p-\frac{\varepsilon_p(L+\frac{V_p}{\varepsilon_c})-(V_D-V_p)}{2K(L+\frac{V_p}{\varepsilon_c})^2}+\left([\frac{\varepsilon_p(L+\frac{V_p}{\varepsilon_c})-(V_D-V_p)}{2K(L+\frac{V_p}{\varepsilon_c})^2}]^2+\frac{(V_D-V_p)I_p}{K(L+\frac{V_p}{\varepsilon_c})^2}\right)^{\frac{1}{2}}\cdots\cdots\cdots\cdots(21)$$

Ⅳ. Comparision of the Model with Measured Data

A comparision of our model with measured data[3] has been performed beginning with the I_{ds}-V_{gs} curves in Fig.3. We observe excellent agreement between the model(dashed line)and measured data(*) for every value of gate voltage. Especially this model gives the realistic description of the subthreshold region of I-V curves in contrast to existing models which are based on only a linear approximation for E_{Fi} shown as a dashed line in Fig.1. Also, we compared I_{Ds}-V_{gs} curves generated by using our improved n_s expression with that generated by the model using the linear approximation $E_{Fi} = a\, n_S + E_{Fio}(KT)$ (dashed line) in Fig.3. Proposed model gives more accurate results even in the linear region of I-V curves which is contributed by the better description of n_S vs E_{Fi} characteristics than the linear approximation for high value of n_s.

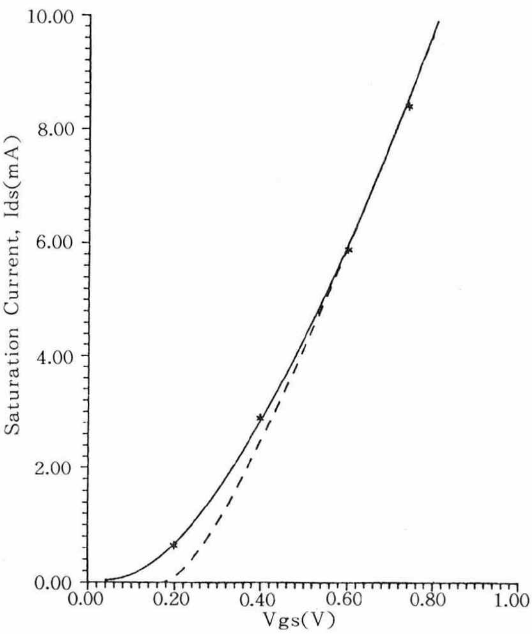

Fig. 3

In order to visualize the behavior of a transconductance in the saturation region of the I-V curves, the derivative of the saturation current with respect to V_g was taken from Eq. 17 and shown in Fig.4. The "*" represents the measured data quoted in [8]and the solid line represents the present model expressed as

$$G_m\big|_{sat} = \frac{\beta V_p}{L + \frac{V_p}{\varepsilon_c}} \left\{ 1 - \frac{\kappa_0 \varepsilon_0}{2Aqd} \left[\left(\frac{B + \frac{\kappa_0 \varepsilon_0}{qd}}{2A} \right)^2 - \frac{1}{A} \left(C - \frac{\kappa_0 \varepsilon_0}{qd} (V_g - V_{th}) \right) \right] \right\}^{-\frac{1}{2}} \qquad (22)$$

Again we find excellent agreement for most of the transconductance characteristics.

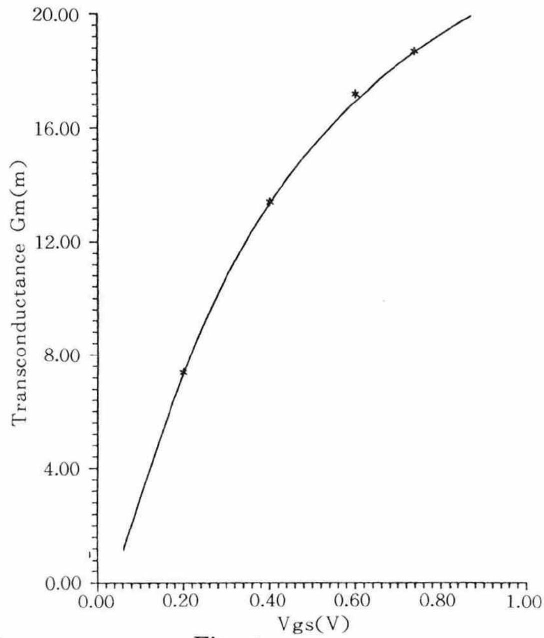

Fig. 4

Finally in Fig. 5, we performed I-V comparison using the same data used above. The device parameters are listed in Table 1. In this comparison the solid line is the present model and the "*"represents measured data both of which are well matched together for all ranges of the terminal voltages. Here we eliminated the device parameter d_S (channel thickness in saturated section under the gate) by expressing it as follows.

Table 1. Device Parameters

Device Parameter	Experimental Data	Model Parameter
$\mu_0(cm^2/V_s)$	4300	2300
vs(m/s)	–	1×10^5
d_d(Å)	300	300
d_i(Å)	100	100
$N_D(cm^{-3})$	1×10^{18}	1×10^{18}
$\triangle E_C$(eV)	–	0.32
ϕb(eV)	–	1.06
Z(μ)	145	145
L(μ)	1	1
$R_S(\Omega)$	12	12
f	–	0.2

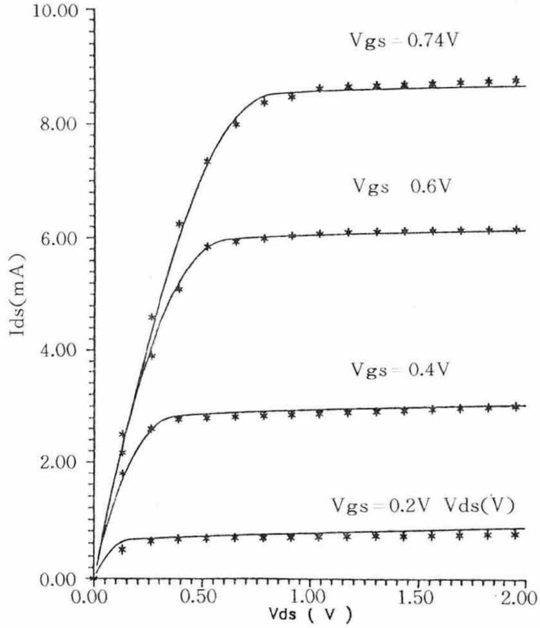

Fig. 5

$$d_s = \frac{\kappa_0 \varepsilon_0}{q} G^{-1}(n_{sP}) \quad \cdots\cdots\cdots (23)$$

where n_{SP} is the channel charge in the saturated section(see Fig.2) evaluating Eq.10 at $V_C = V_P$

$$n_{sp} = \frac{\kappa_0 \varepsilon_0}{qd} \{ V_g - V_{th} - (1-f) V_p - \frac{E_{Fi}(V_g)}{q} \} \quad (25)$$

Our I - V simulation reveals that the low field mobility $\mu 0$, source access resistance Rs, and f parameter are closely linked togeter

V . Conclusion

Completely closed form analytical model for HEMT was discussed. The continous charge control model describing nonlinear behavior of the 2-DEG including subthreshold region was incorporated. A transconductance comparison was performed to verify the model. This will provide fast and accurate device model for HEMTs circuit simulators. In near future, parasitic MESFET region and nonlinear source resistance model will be published.

REFERENCES

1. D. Delagebeardeuf and N. T. Linh, "Metal-(n) AlGaAs-GaAs two-dimensional electron gas FET", *IEEE Trans, Electron Devices*, vol. Ed-29, pp.955-960, June 1982.
2. Young Min Kim and P.Roblin, "Two-Dimensional Charge Control Model for MODFETs", *IEEE Trans. on Electron Devices*, vol. 22, Nov.1986.
3. K. Lee et al., "Current-Voltage and Capacitance-Voltage characteristics of Modulation-Doped Field-Effect Transistors", *IEEE Trans. Electron Devices*, vol. ED-30, No.
4. Young Min Kim, "A Two-Dimensional charge control model and an analytical CAD model for MODFET's *Ph.D.Dissertation*, Electrical Engineering, Ohio State University Dec. 1986.
5. Kwangmean Park and Kae Dal Kwack, "A model for the current-voltage characteristics of MODFET's", *IEEE Trans. Electron Devices*, Vol ED-33, No.5, May 1986.
6. H.Morkoc, "High speed modulation-doped AlGaAs/GaAs field effect transistors : MODFETs) ; analysis, fabrication and performance", Internal Reports, Department of Electrical Engineering and Coordinated Science Laboratory, Univ. of Illinois.
7. Young Min Kim, "An Analytical DC Model for HEMT's, "*Journal of KITE*, Vol. 26, No.6, June 1989.

8. Chian S. Chang and Harold R. Fetterman, "An Analytical Model for High-Electron-Mobility Transistors", *Solid-States Electronics,* Vol.26, No.6, June 1987.

金 榮 民 (Kim, Young Min)

1976. 2 : 서울대학교 전자공학과 학사
1978. 2 : 한국과학원 전기 및 전자 공학과 석사
1978. 3 : 한국 선박 해양 연구소 전산실
1979. 8 : 국방과학연구소(ADD)
1986.12 : 미국 Ohio State University 전기공학과 박사
1987. 1 : 미국 North Carolina A&T State University 전기공학과 조교수
1988. 6 ~ 현재 : 한국전자통신연구소 통신소자개발실장